



HAL
open science

Thermal Polymerization on the Surface of Iron Oxide Nanoparticles Mediated by Magnetic Hyperthermia: Implications for Multi-Shell Grafting and Environmental Applications

Nébéwia Griffete, Jérôme Fresnais, Ana Espinosa, Dario Taverna, Claire Wilhelm, Christine Ménager

► To cite this version:

Nébéwia Griffete, Jérôme Fresnais, Ana Espinosa, Dario Taverna, Claire Wilhelm, et al.. Thermal Polymerization on the Surface of Iron Oxide Nanoparticles Mediated by Magnetic Hyperthermia: Implications for Multi-Shell Grafting and Environmental Applications. ACS Applied Nano Materials, 2018, 10.1021/acsanm.7b00063 . hal-01685470

HAL Id: hal-01685470

<https://hal.sorbonne-universite.fr/hal-01685470>

Submitted on 16 Jan 2018

HAL is a multi-disciplinary open access archive for the deposit and dissemination of scientific research documents, whether they are published or not. The documents may come from teaching and research institutions in France or abroad, or from public or private research centers.

L'archive ouverte pluridisciplinaire **HAL**, est destinée au dépôt et à la diffusion de documents scientifiques de niveau recherche, publiés ou non, émanant des établissements d'enseignement et de recherche français ou étrangers, des laboratoires publics ou privés.

Thermal Polymerization on the Surface of Iron Oxide Nanoparticles Mediated by Magnetic Hyperthermia: Implications for Multi-Shell Grafting and Environmental Applications

Nebewia Griffete^{†}, Jérôme Fresnais[†], Ana Espinosa[‡], Dario Taverna[§], Claire Wilhelm[‡], and
Christine Ménager[†]*

[†] Sorbonne Universités, UPMC Univ Paris 06, CNRS, Laboratoire PHENIX, Case 51, 4 place
Jussieu, F-75005 Paris, France.

Email: nebewia.griffete@upmc.fr

[‡] MSC, UMR CNRS 7057, University Paris Diderot, 75205 Paris cedex 13, France.

[§] Institut de Minéralogie, de Physique des Matériaux et de Cosmochimie (IMPMC), Sorbonne
Universités - UPMC Univ. Paris 6, CNRS UMR 7590, IRD UMR 206, MNHN, 4 place Jussieu,
F-75005 Paris, France.

Keywords: Radical surface polymerization, synthesis, alternating magnetic field, polymer,
molecularly imprinted polymer, magnetic nanoparticles.

ABSTRACT: A fast and straightforward strategy for thermo-polymerization of polymer shells,
at room temperature, at magnetic nanoparticles (MNP) surface under alternating magnetic field

(AMF) is presented. The polymerization is triggered by the local heat generated by the MNP when exposed to AMF to polymerize an organic shell around the MNP by thermo-activation. This synthetic approach provides a versatile strategy for magnetic nanoparticles surface polymerization without macroscopic temperature increase, allowing efficient pathways to magnetically induce single layer by layer polymer shells. This method provides an unprecedented multifunctional nanoplatfrom adapted to pollutant targeting by using molecularly imprinted polymer layer polymerized at room temperature.

1. INTRODUCTION

Magnetic nanoparticles (MNP) have been the subject of extensive research during the last decade because of their potential applications in many fields such as diagnostic,^{1,2} nucleic acid separation,^{3,4} drug delivery⁵⁻⁹ or even for environmental pollutants removal.^{10,11} They have attracted considerable attention for hyperthermia applications, owing to their ability to generate heat when exposed to an alternating magnetic field (AMF).¹²⁻²⁰ However, iron oxide nanoparticles are rarely used without coating protection due to their easy aggregation, their quick biodegradation, and their further loss of magnetic properties.^{21,22} The iron oxide surface is usually modified with an inorganic layer,²³⁻²⁵ such as silica, metal oxide or metal sulfide or by the grafting of organic molecules, including surfactants, biomolecules or polymers^{26,27} such as polyacrylic acid²⁸ or dextran.²⁹ Therefore, to keep the stability of magnetic iron oxide NP, it is important to provide a surface with good chemical stability and new methods on the development of coating is of special interest.

Recently, Haupt et al. proposed an original strategy for coating upconverting nanoparticles (UCP) with polymer shells by using the particles as internal light sources.³⁰ The method used the

UV or visible light emitted from UCP upon photoexcitation with near-infrared radiation, to locally photopolymerize a thin polymer shell around the UCP. Based on this work, it should be possible to initiate the polymerization from magnetic nanoparticles surface by using their heating properties under alternating magnetic field. Darwish et al. used AMF to heat a magnetic powder dispersed in PDMS particles to speed up the crosslinking of SYLGARD 184.³¹ However, they do not initiate the polymerization under AMF. Only one theoretical study, based on molecular dynamic simulations, showed the feasibility to use an alternating magnetic field to induce polymerization via the decomposition of a magnetic macro-initiator.³²

In this paper, we demonstrate for the first time that AMF can be used to trigger the polymerization directly at the surface of MNP which act as nanoheaters. A thin shell of acrylamide is grown by thermopolymerization around the MNP followed by a second shell made of molecularly imprinted polymer (MIP).³³⁻³⁸ As a proof of concept, these core-shell-shell nanoparticles with specific molecule recognition ability, are used for concentration of pollutants. This easy to handle synthesis represents a generic process to create a stable cross-linked polymer coating on MNP, with a large choice of functional groups, without macroscopic heating. This could be of utmost importance when MIP are synthesized with thermosensitive templates such as proteins.

2. EXPERIMENTAL DETAILS

2.1. Materials. Acetonitrile (99.8%), ethanol (99.8%), hydrochloric acid (37%), nitric acid (52%), iron (III) nitrate nonahydrate ($\text{Fe}(\text{NO}_3)_3 \cdot 9\text{H}_2\text{O}$, 99%), iron(III) chloride hexahydrate ($\text{FeCl}_3 \cdot 6\text{H}_2\text{O}$, 97%), acetone, ether, methacrylic acid (MAA), acrylamide (AM), paranitrophenol (PNP), phenol, 4-nitroaniline (4-NA), *N,N'*-Methylenebisacrylamide (MBAm), 2-(dodecylthiocarbonothioylthio)-2-methylpropionic acid (TTMA) from Sigma-Aldrich were used

as received. Iron(II) chloride tetrahydrate ($\text{FeCl}_2 \cdot 4\text{H}_2\text{O}$, 98%), Azobisisobutyronitrile (AIBN), ammonia (20%) were purchased from Acros.

2.2. Maghemite nanoparticles synthesis. ($\gamma\text{-Fe}_2\text{O}_3$) were synthesized by coprecipitation of Fe^{3+} and Fe^{2+} ions according to Massart's procedure.³⁹ Magnetite (Fe_3O_4) nanocrystals were prepared by coprecipitation of FeCl_3 (1.6 mol) and $\text{FeCl}_2 \cdot 4\text{H}_2\text{O}$ (0.9 mol) salts in alkaline solution (NH_4OH , 7 mol). The solid phase was separated from the supernatant by magnetic separation and immersed in a boiling solution (100 °C) of ferric nitrate ($\text{Fe}(\text{NO}_3)_3$, 0.8 mol) during 30 minutes to completely oxidize magnetite into maghemite ($\gamma\text{-Fe}_2\text{O}_3$). After magnetic decantation, 2 L of distilled water and 360 mL of HNO_3 20% were added to the solution and the mixture was stirred for 10 min. After washing steps in acetone and diethyl-ether to remove the excess of ions, as prepared maghemite nanoparticles were suspended in water (1L) at pH 1.5. To get the largest NP, 20 mL of HNO_3 (68%) were added to the solution and the mixture was stirred during 10min. A dense phase containing the big particles was separated from the supernatant containing the small ones. The dense phase was washed twice with acetone (200 mL) and twice with diethyl ether (200mL). Then 100 mL of water was added for the final dispersion.

The volume fraction and average size of the maghemite NP were determined by fitting the magnetization curve using Langevin's law. The magnetic size of the particles was also measured by TEM. The final iron content was checked by atomic absorption spectroscopy (AAS , $C_{\text{Fe}} = 6.1 \text{ mol.L}^{-1}$) after degradation of the nanoparticles in acidic media (boiling HCl 35%).

2.3. Surface modification. The surface of $\gamma\text{-Fe}_2\text{O}_3$ NP was then modified with TTMA by the following procedure. Two milliliters of the suspension ($[\text{Fe}] = 6 \text{ mol.L}^{-1}$) was added to a 100 mL mixture of water/ethanol (v/v 3/7) under ultrasonication during 10 min at room temperature, followed by the addition of 0.1 g of TTMA (0.27 mmol). We choose a water/ethanol solvent

because it allows the dispersion of the NPs and the solubilization of TTMA. The mixture was shaken at a rate of 300 rpm for 24 h. The final product of Fe₂O₃@TTMA was separated and purified by magnetic collection and washed with ethanol and deionized water for three times. The presence of TTMA at the surface of Fe₂O₃ NP was evidenced by Fourier transform infrared (FT-IR) spectroscopy. The DLS measurement (Figure S1) of the magnetic nanoparticles modified with TTMA showed a larger size distribution in water after their surface modification. As this ligand is hydrophobic, in water the particles seem to aggregate.

2.4. Polymerization. Acrylamide and MBAm were used as the functional monomer and cross-linking agent of the polymerization respectively. Five milliliters of the suspension containing Fe₂O₃@TTMA NP ([Fe] = 0.05 M) was mixed with acrylamide (7 mmol), MBAm (28 mmol) and 5 mg of AIBN (0.03 mmol) as the polymerization initiator. The mixture was purged with nitrogen for 10 min and then the polymerization could proceed in a mixture of water/ethanol^{40,41} by applying AMF at different frequencies (144, 214, 342, 470 kHz) and different magnetic field intensities (4.8, 9, 13.5 and 18 mT) at 25 °C for 10min. It is possible that some polymer chains were formed in solution. As we use a crosslinker, we cannot analyze by steric exclusion chromatography, after magnetic decantation, the supernatant that may contain free polymer chains. The final product consisting of Fe₂O₃@PAM NP was dialyzed during 24 hours with a standard regenerated cellulose membrane (6000 g.mol⁻¹ MWCO), washed several times by magnetic separation (the supernatant is eliminated) using ethanol as non-solvent and finally dispersed in water to be sure that at the end of the washing steps there is no polymer in solution.. To prove the surface initiation of the polymerization under AMF, the same polymerization was realized (9mT, 342 kHz) without TTMA as transfer agent. The dynamic light scattering (DLS) seems to show-no increase in size after polymerization (Figure S2).

Fe₂O₃@PAM@MIP-PNP NP were synthesized by using the same procedure. A solution containing Fe₂O₃@PAM NP, paranitrophenol (PNP, 0.28 mmol), methacrylic acid (MAA, 0.554 mmol), MBAm (2.76 mmol) in a mixture of water/ethanol (v/v 3/7) was purged with nitrogen for 10 min and then AMF was applied for 10 min. We chose a value of 1/4 for the ratio functional monomer/crosslinker as usually used for MIP synthesis. After polymerization, the nanoparticles were washed in methanol/acetic acid (9:1) and with ethanol, to eliminate PNP. Then the final product consisting of Fe₂O₃@PAM@MIP NP was dialyzed during 24 hours with a membrane of 6000 g.mol⁻¹ MWCO, washed several times by magnetic separation and finally dispersed in water.

2.5. Adsorption and release experiments. Isothermal adsorption experiments were carried out during 3 hours for Fe₂O₃@PAM@MIP and Fe₂O₃@PAM@NIP (NIP for Non Imprinted Polymer, the polymer without the paranitrophenol imprint) (20 mg) through varying the concentrations of PNP from 0.4 to 5.2 mg.L⁻¹ in water at pH 5.5. After 3h incubation, the supernatant (3mL) was separated from the magnetic particles using a magnet and the amount of free PNP was quantified by UV-visible spectrophotometry. The PNP concentration was measured in basic conditions (pH = 10). At this pH, phenolate functions exhibit a typical yellow color and absorb at 400 nm. We calculated the PNP concentration by using the absorption coefficient $\epsilon = 18103 \text{ L.cm}^{-1}.\text{mol}^{-1}$ (Figure S3). To determine the binding selectivity of Fe₂O₃@PAM@MIP for PNP, isothermal adsorption experiments were carried out through varying the concentrations of 4-nitroaniline and phenol from 0.3 to 5 mg.L⁻¹ during 3 hours. The supernatant was then analyzed by UV-visible spectrophotometry.

PNP kinetic release study was monitored at 25 °C under an alternating magnetic field pulse of 10, 15, 20, 25 and 30 min (342 kHz, 9 mT). At each time point the Fe₂O₃@PAM@PNP-MIP (3

mL, 20 mg) particles were dialyzed and the supernatant was analyzed by UV-visible spectrophotometry to quantify the amount of molecule released.

For the material regeneration, the $\text{Fe}_2\text{O}_3@\text{PAM}@MIP$ NP (3 mL, 20 mg) were recovered and mixed with a PNP solution ($6 \text{ mg}\cdot\text{L}^{-1}$) during 1h. Then the supernatant was collected by UV/Vis spectroscopy to confirm the successful PNP adsorption. Three adsorption- release cycles were performed on the same sample.

2.6. Characterizations. The TEM analysis was performed using a Jeol-100 CX TEM. A droplet of diluted nanoparticles suspension in water was deposited on a carbon coated copper grid and the excess was drained using a filter paper. Size analysis was achieved on TEM images using ImageJ software.

High resolution transmission electron microscopy (HRTEM) and Electron filtered transmission electron microscopy (EFTEM) were performed on a JEOL 2100F microscope, equipped with a Gatan GIF 2001 spectrometer for energy-filtered imaging.

Hydrodynamic diameter (d_h) measurements were performed by DLS with a Malvern Instruments Nanosizer.

Magnetic properties of the iron oxide nanoparticles were measured by vibrating sample magnetometer at room temperature.

Fourier Transform Infra-Red spectra of Fe_2O_3 , $\text{Fe}_2\text{O}_3@TTMA$, and polymer modified Fe_2O_3 nanoparticles were recorded on a Bruker Tensor 27 spectrometer on pressed KBr pellets. Spectra were obtained at regular time intervals in the MIR region of $4000 - 400 \text{ cm}^{-1}$ at a resolution of 4 cm^{-1} and analyzed using OPUS software.

Hyperthermia experiments for nanoparticles in suspension were conducted on a commercial magneTherm apparatus (magneTherm AC system, Nanotherics Corp) with different frequencies and fields. The temperature was probed using a fluoro optic fiber thermometer.

Absorbance measurements were done with an Avantes UV-visible spectrophotometer, with 100 μm optical fibers. UV/VIS measurements were configured with a range from 200 to 1100 nm. A combined deuterium-halogen light source was used.

The total iron concentration (mol.L^{-1}) was determined by atomic absorption spectroscopy (AAS) with a Perkin-Elmer Analyst 100 apparatus after degradation of $\gamma\text{-Fe}_2\text{O}_3$ NP in boiling HCl (35%).

3. RESULTS AND DISCUSSION

3.1. Heating efficiency of MNP. The objective of the work consists of the polymerization, from the surface of iron oxide nanoparticles, induced by the local heating under alternating magnetic field. As the polymerization initiation is only located at the surface, the global macroscopic temperature should not increase. The maghemite ($\gamma\text{-Fe}_2\text{O}_3$) NP were first synthesized by a coprecipitation method, followed by a size sorting process through salt destabilization to get the largest NP, most efficient for magnetic hyperthermia.^{42,43}

TEM and HRTEM pictures (Figure 1A) shows particles with an average particle diameter (d_0) of 10 nm ($\sigma = 0.29$, following a lognormal distribution) and clear lattice fringes. The particles exhibit a superparamagnetic behavior (Figure S4).

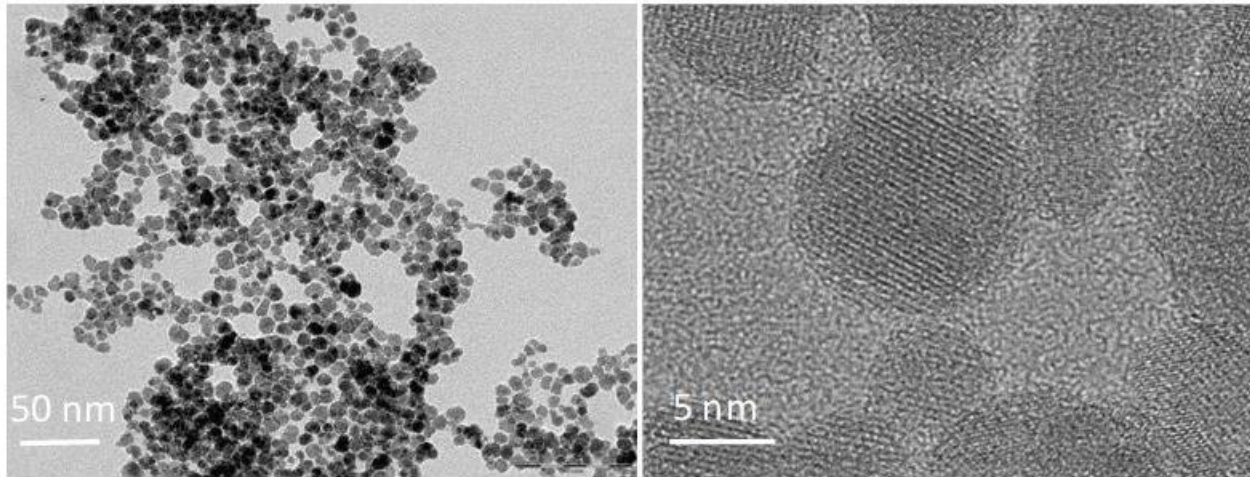


Figure 1. TEM images and high resolution TEM images of $\gamma\text{-Fe}_2\text{O}_3$. TEM images show particles with an average particle diameter (d_0) of 10 nm and a polydispersity σ of 0.36.

The heating efficiency of the iron oxide nanoparticles core ($[\text{Fe}] = 50 \text{ mM}$, 300s AMF application at 25°C with magnetic field intensity of 18 mT, Figure 2a and b) was measured at different frequencies (144, 214, 342, 470 kHz) and different magnetic field intensities (4.8, 9, 13.5 and 18 mT). The heating power is expressed in terms of specific absorption rate (SAR). It is obtained from the initial slope of temperature curves⁴⁴ and it varies with the external magnetic field parameters. As shown in Figure 2c and d, SAR increases with the amplitude and frequency of the magnetic field. At low frequency (144 kHz) the macroscopic temperature doesn't increase but at 342 and 470 kHz the temperature reaches 31 and 34.5°C (starting temperature is about 25°C), respectively, lower than the temperature usually needed to initiate the polymerization (60°C). These three frequencies will be tested to initiate the polymerization.

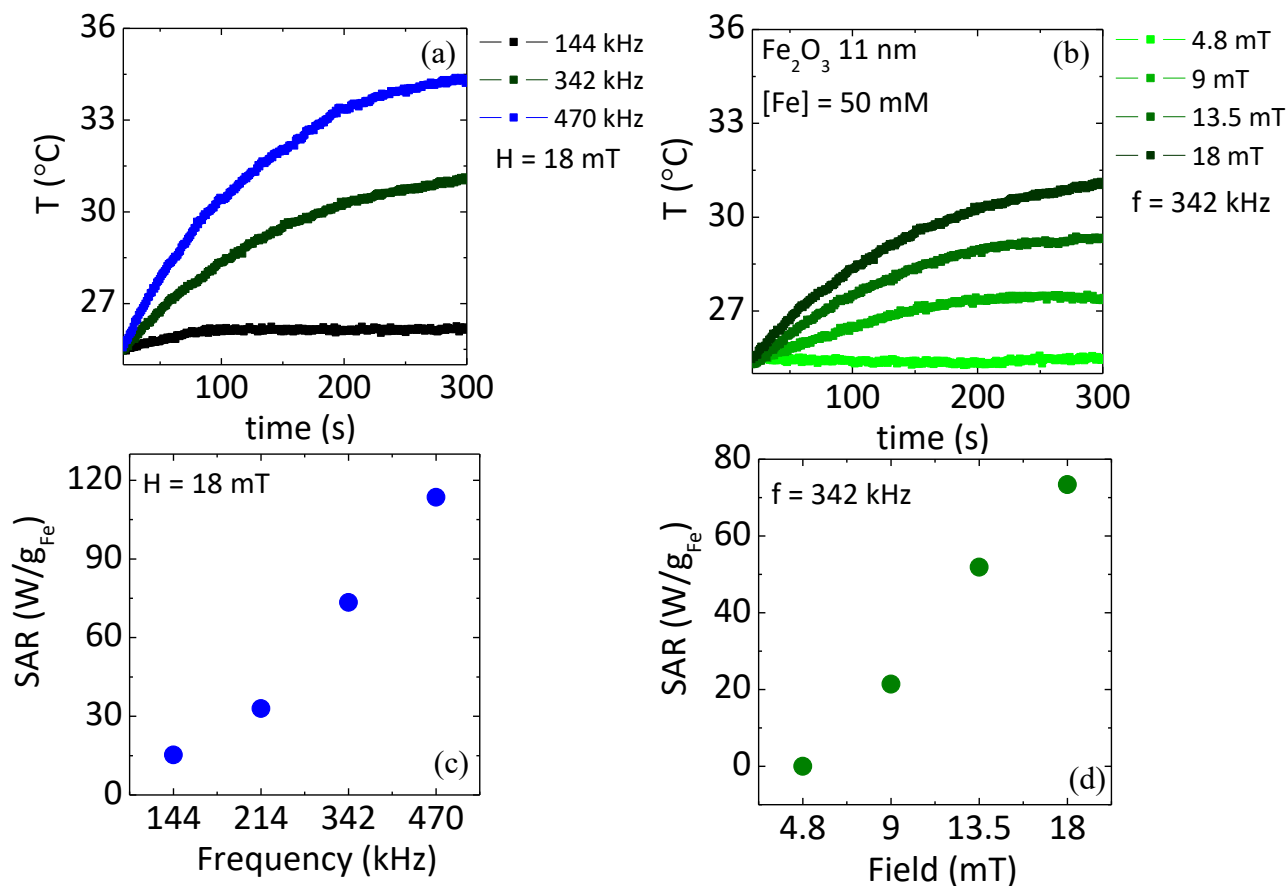


Figure 2. Temperature variation of γ -Fe₂O₃ NP (2 mL, [Fe] = 0.05 mol L⁻¹) under AMF a) at H = 18mT and different frequencies (144, 214, 342, 470 kHz) and b) at 342 kHz and different magnetic field intensities (4.8, 9, 13.5 and 18 mT). (c) and (d) represent the heating efficiency (SAR, in W per gram of iron) of γ -Fe₂O₃ NP (2 mL, [Fe] = 0.05 mol L⁻¹) under AMF.

3.2. Synthesis of Fe₂O₃@PAM NP. We prepared Fe₂O₃@polymer NP following the process illustrated in Figure 3 and explained in the materials and methods section. The surface of the nanoparticles is modified with 2-(dodecylthiocarbonothioylthio)-2-methylpropionic acid (TTMA) for surface-initiated polymerization (SIP). SIP on iron oxide NP was ever achieved by grafting an ATRP initiator or a nitroxide for NMP synthesis at the surface of size-sorted iron oxide NPs. The control of polymerization was demonstrated by degrading the iron oxide cores in HCl and by analyzing the (de-grafted) chains by GPC.^{45,46} Here, the strategy relies on the use of a

bifunctional transfer agent containing a functional end group for surface anchoring (carboxylic acid)^{47,48} and a trithiocarbano function able to activate the SIP. Then, the polymerization could proceed, mixing Fe₂O₃TTMA nanoparticles with acrylamide as the functional monomer, *N,N*-Methylenebis(acrylamide) (MBAm) as the crosslinking agent, and azo(bis)isobutyronitrile (AIBN) as the polymerization initiator in a mixture of ethanol/water (3:7). The amount of radical initiator AIBN added is calculated accordingly to the TTMA quantity used in the synthesis (after verification that all the TTMA anchored to the surface, we used a ratio of TTMA /AIBN of 9/1 even if the usual ratio between TTMA and AIBN is 5/1 or 7/1).^{49,50} The deoxygenated mixture was placed under AMF (18 mT) for 10 min at different frequencies (144, 342 and 470 kHz) to determine the optimal frequency to initiate the polymerization. The final product, consisting of nanoparticles coated by a polyacrylamide shell (Fe₂O₃@PAM), was dialyzed during 24 hours against water. The produced Fe₂O₃@PAM NP were dispersed in water at pH 5.5.

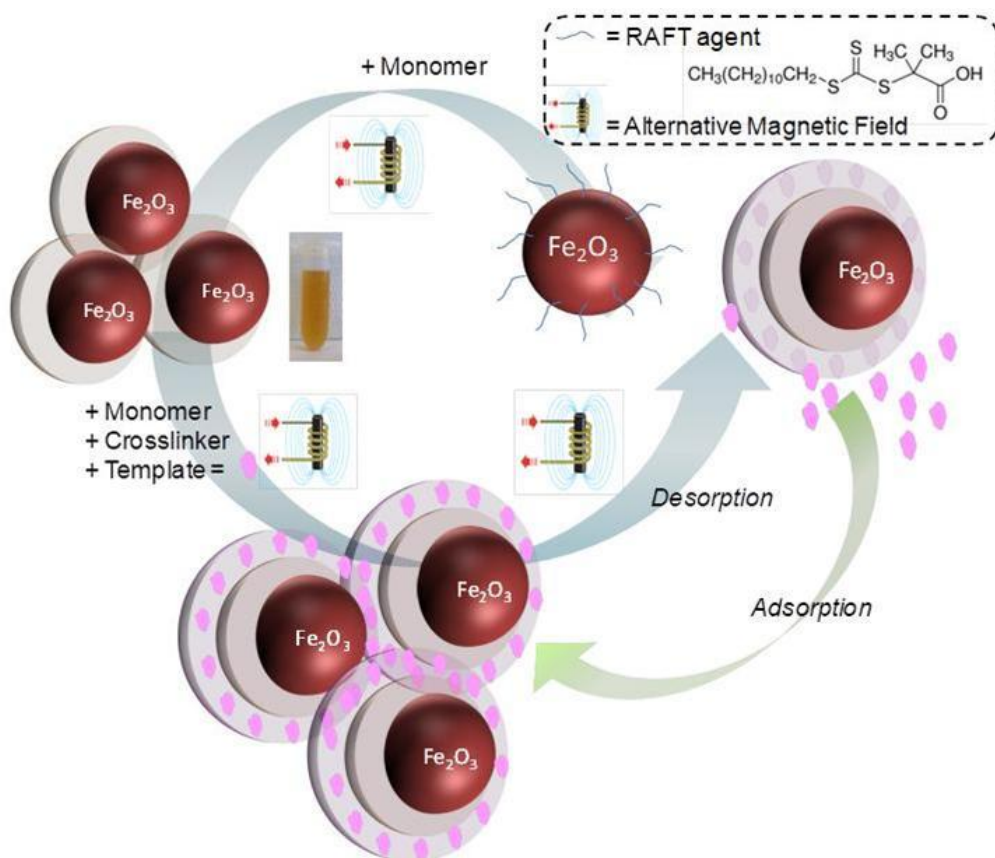


Figure 3. Principle of the magnetic hyperthermia induced polymerization for shell grafting. The heat produced by the magnetic nanoparticles, when excited under alternating magnetic field, is exploited to create a polymeric shell in situ around the nanoparticle by thermopolymerization. A second shell, in our case, a molecularly imprinted polymer (MIP), can be grafted as well by re-initiation in the presence of different monomers and a molecular template. AMF can also be used for molecule desorption, by disrupting hydrogen bonds, when synthesizing a MIP.

HRTEM images of Fe₂O₃@PAM synthesized under AMF (342 kHz, 9 mT, Figure 4Ai) reveal the presence of an amorphous polymer around well crystallized γ -Fe₂O₃ NP. The chemical nature of the amorphous shell was analysed by energy-filtered transmission electron microscopy (EFTEM, Figure 4Ai and ii). Elemental signal of carbon (in white) was detected at the surface and at the interspace between particles (Figure 4Aiii) indicating the presence of the polymer around the magnetic nanoparticles. Finally, TEM confirms the presence of an amorphous shell around the MNP when the polymerization is done under AMF.

The polyacrylamide shell of Fe₂O₃@PAM is evidenced by IR spectroscopy (Figure 4B) with the presence of new peaks compared to particles before polymerization detected at 3455 (NH₂), 2904 (CH₂), 1746 cm⁻¹ (C=O).⁵¹ If we compare their IR spectra intensity of CH₂ peak (2904 cm⁻¹) (FeO peak as reference^{52,53}) we found that the more intense bands are obtained for the nanoparticles synthesized using a 342 or 470 kHz frequency at 18mT (Figure S5).

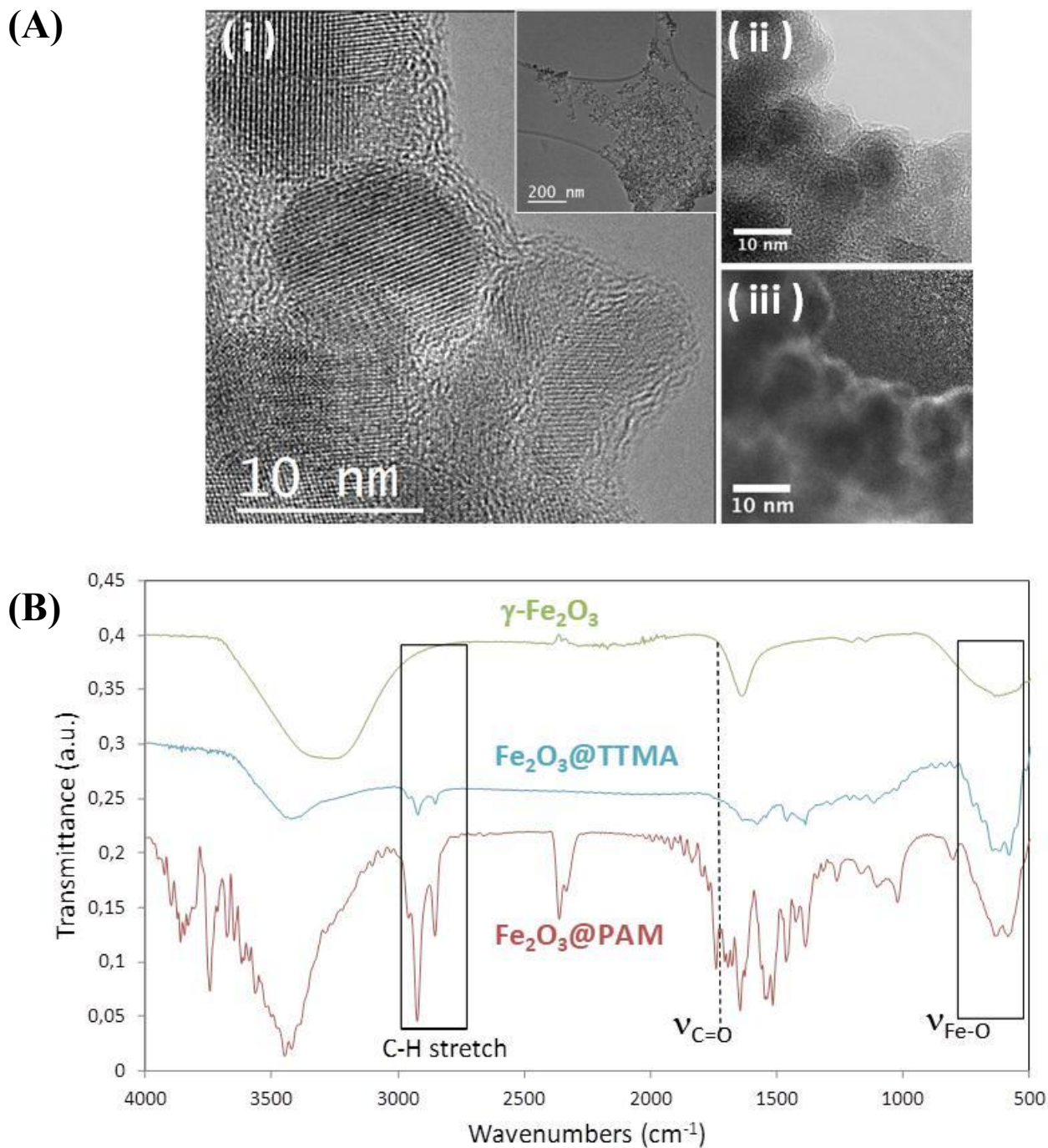


Figure 4. A) HRTEM images of polyacrylamide modified iron oxide nanoparticles synthesized under AMF $f=342$ kHz, $H = 9$ mT for 10 min. Inset: (i) EFTEM analysis of $\text{Fe}_2\text{O}_3@PAM$ showing a conventional TEM image (ii) and elemental mapping of carbon (iii). B) FT-IR spectra of $\gamma\text{-Fe}_2\text{O}_3$, $\text{Fe}_2\text{O}_3@TTMA$ and $\text{Fe}_2\text{O}_3@PAM$.

As the polymerization is effective at 342 kHz with minimal macroscopic temperature increase (31°C), we chose this frequency for the following. Additionally, as the IR spectra are almost the same at 342kHz, 18mT and 342kHz, 9mT (Figure S6), we decreased the intensity of the magnetic field to 9mT to further minimize the macroscopic temperature elevation (less than 2°C, see Figure 2Bb) during polymerization.

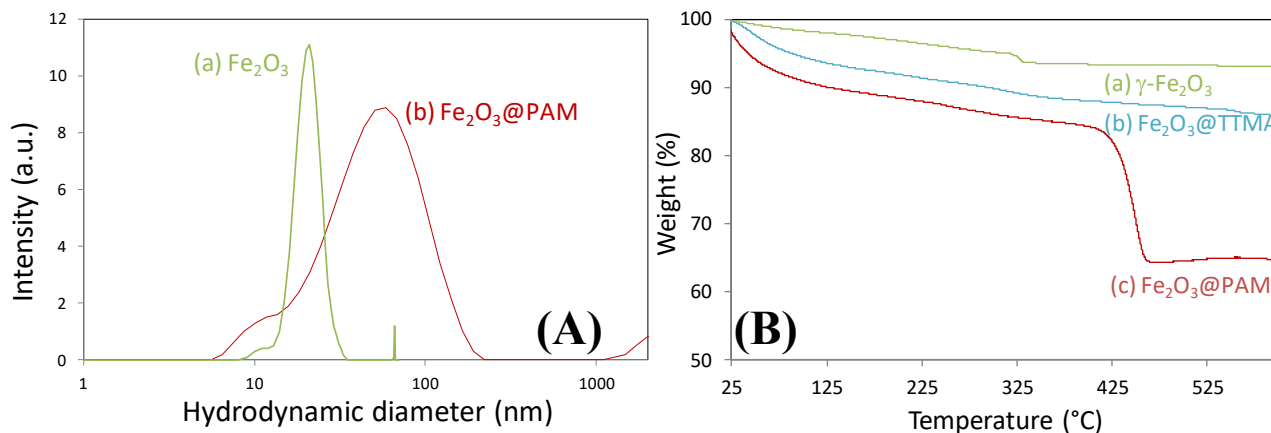


Figure 5. A) Hydrodynamic diameter measured by DLS (intensity average) of (a) Fe_2O_3 and (b) $\text{Fe}_2\text{O}_3@PAM$ NP diluted respectively in acidic water and in water at a concentration of approximately $0.05 \text{ mol}\cdot\text{L}^{-1}$. B) Thermogravimetric analysis of (a) Fe_2O_3 (b) $\text{Fe}_2\text{O}_3@TTMA$ and (c) $\text{Fe}_2\text{O}_3@PAM$ NP.

The presence of a polymer shell is also evidenced by the increase of the hydrodynamic diameter after polymerization as illustrated by dynamic light scattering (DLS) measurements, revealing an increase from 27 (zeta potential = 32 mV)⁵⁴ to 58 nm (PDI = 0.28 and 0.66) for $\gamma\text{-Fe}_2\text{O}_3$ and $\text{Fe}_2\text{O}_3@PAM$, respectively (Figure 5A). The presence of a bimodal curve may be due to the presence of NP population with polymer shell thicker or due to partial aggregation (10 particles).

Finally, thermogravimetric analysis (TGA) shows that the amount of TTMA was about 14% of the total particles weight (as expected from the synthesis described in part 2.3) and the amount

of PAM on $\text{Fe}_2\text{O}_3@\text{PAM}$ was about 38% of the total particle weight, as determined from the significant mass change between 420 and 470 °C owing to decomposition of PAM (Figure 5B). Additionally, the nanoparticles remain dispersed (see photo Figure 1 and DLS Figure S7), even after 1 year, evidencing the steric stabilization provided by the polymer overlayer.

We used three different durations of polymerization (10, 20 and 30 minutes, 342kHz, 18mT) but as the polymer is ever present after 10 minutes of polymerization (see IR spectra in figure S8) we used this time for the rest of the experiments.

3.3. Comparison with a bulk heating. We decided to synthesize $\text{Fe}_2\text{O}_3@\text{PAM}$ NP in a water bath at 60°C during 10min (labeled $\text{Fe}_2\text{O}_3@\text{PAM}_T$) and to compare this synthesis to the one obtained under AMF (342kHz, 9mT, 10 min) labeled $\text{Fe}_2\text{O}_3@\text{PAM}_{AMF}$.

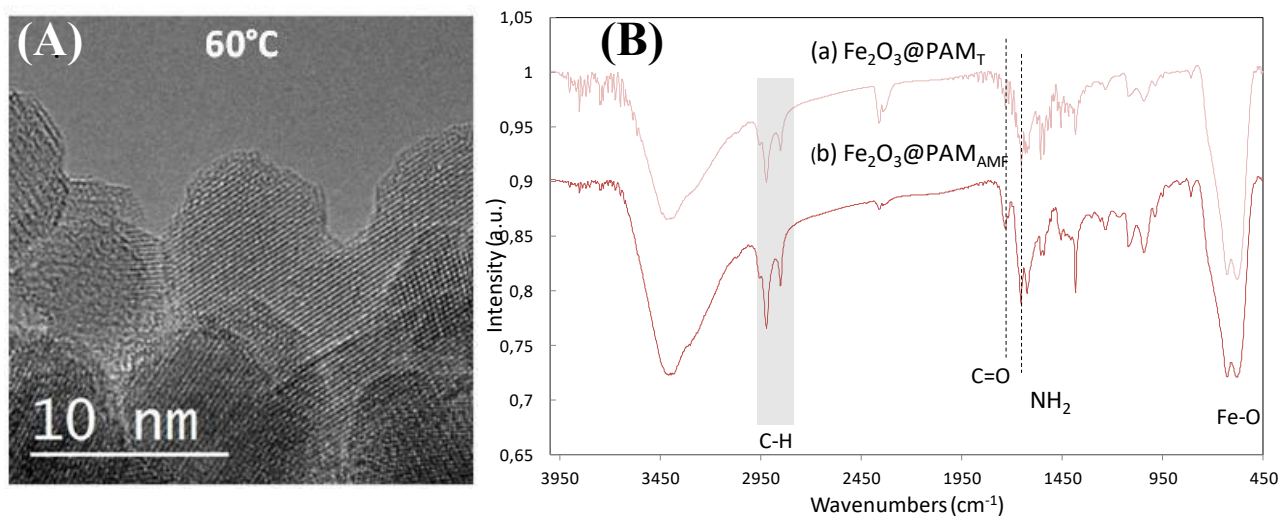


Figure 6. A) HRTEM image of $\text{Fe}_2\text{O}_3@\text{PAM}_T$ synthesized at 60°C. B) FT-IR spectra of (a) $\text{Fe}_2\text{O}_3@\text{PAM}_T$ nanoparticles and (b) $\text{Fe}_2\text{O}_3@\text{PAM}_{AMF}$.

No amorphous shell seems to be observed for the $\text{Fe}_2\text{O}_3@\text{PAM}_T$ (Figure 6A and S9b) on HRTEM images.

Additionally, the IR spectra of $\text{Fe}_2\text{O}_3@\text{PAM}_T$ exhibit the same new peaks after polymerization than $\text{Fe}_2\text{O}_3@\text{PAM}_{\text{AMF}}$ but their intensities are lower than the ones of the polymer synthesized under AMF (Figure 6B). This result is in agreement with the TEM results where no (or a thin) polymer shell is visible. At equal reaction times, the AMF induced polymerization is more efficient. However, the macroscopic temperature of the polymerization medium under AMF (31°C) is too low to induce the polymerization, but the temperature generated at the surface of MNP under AMF was estimated to be larger than 60°C , for instance through the use of fluorophores as molecular thermometers at the nanometer scale.^{55,56} For the same kind of MNP, the local temperature was estimated around 60°C as previously published.⁷ This temperature is sufficient to activate the polymerization initiation through AIBN decomposition. In conclusion, under AMF, as the temperature increase is located only around the iron oxide nanoparticles, the polymer can be formed faster than with a standard method, and in a more homogeneous way. AMF is well known to heat magnetic nanoparticles and we tried the polymerization under AMF under the same conditions that those used for $\text{Fe}_2\text{O}_3@\text{PAM}$ NP but without magnetic nanoparticles and we saw no temperature increase and no polymer in solution (no peak in DLS). For these reasons, we claim that the polymerization is induced thanks to AMF.

3.4. Thermopolymerization of a second shell with specific adsorption properties. The second step towards a versatile nanoplatform is to thermopolymerize a second functional shell by using the same localized heating generated by the magnetic cores under AMF that could present removal pollutants properties. For this purpose, we chose the molecular imprinting technique that is used to create artificial imprint by the formation of a polymer network around a template molecule⁵⁷⁻⁵⁹. We synthesized a molecularly imprinted polymer on the $\text{Fe}_2\text{O}_3@\text{PAM}$ under AMF (10 min 342 kHz, 9 mT) in a MIP polymerization mixture containing paranitrophenol (PNP)

methacrylic acid (MAA), and the macroinitiator $\text{Fe}_2\text{O}_3@\text{PAM}$ NP that still possess ending transfer agent functions. PNP is a micropollutant widely used in the production of pesticides which caused great harm to the environment and humans.

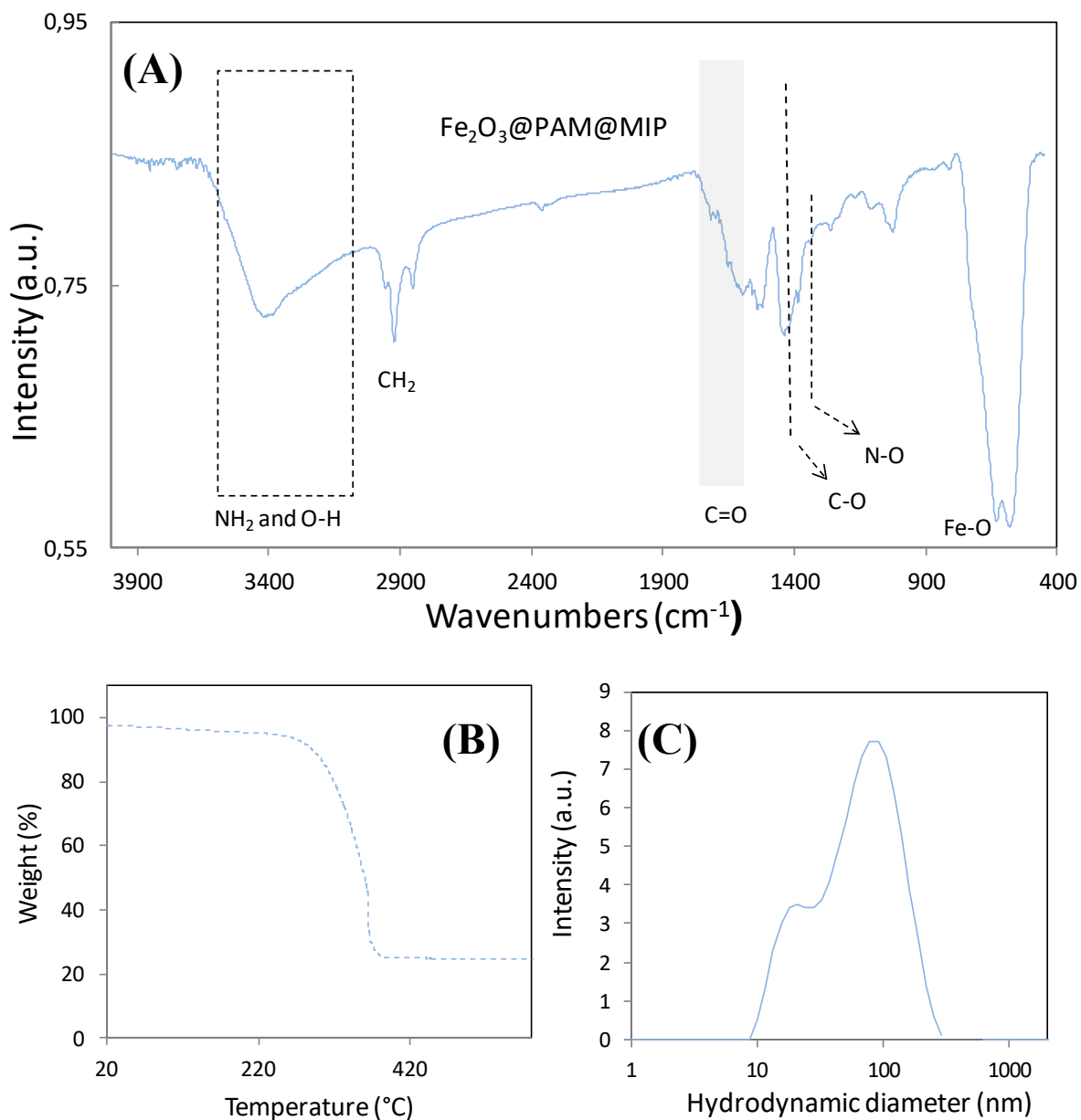


Figure 7. A) FT-IR spectra B) Thermogravimetric analysis and C) Hydrodynamic diameter (intensity average, PDI = 0.64) measured by DLS (in water at a concentration of approximately 0.05 mol.L^{-1}) of $\text{Fe}_2\text{O}_3@\text{PAM}@MIP$ nanoparticles.

After polymerization, the PNP was extracted (labeled $\text{Fe}_2\text{O}_3@\text{PAM}@MIP$) and IR spectra (Figure 7A), TGA (Figure 7B) and DLS (Figure 7C) show respectively the increase of the intensities of the C=O and CH_2 peaks, the significant mass change (from 38 to 63% of the total particle weight), and the increase of the two population hydrodynamic diameter. The same procedure was applied to non-imprinted (NIP) magnetic nanoparticles, which were prepared in the same way as the MIPs, but in the absence of the PNP template. The TGA (Figure S10) shows the same significant mass change than the $\text{Fe}_2\text{O}_3@\text{PAM}@MIP$ NP confirming the efficiency and reproducibility of the polymerization method.

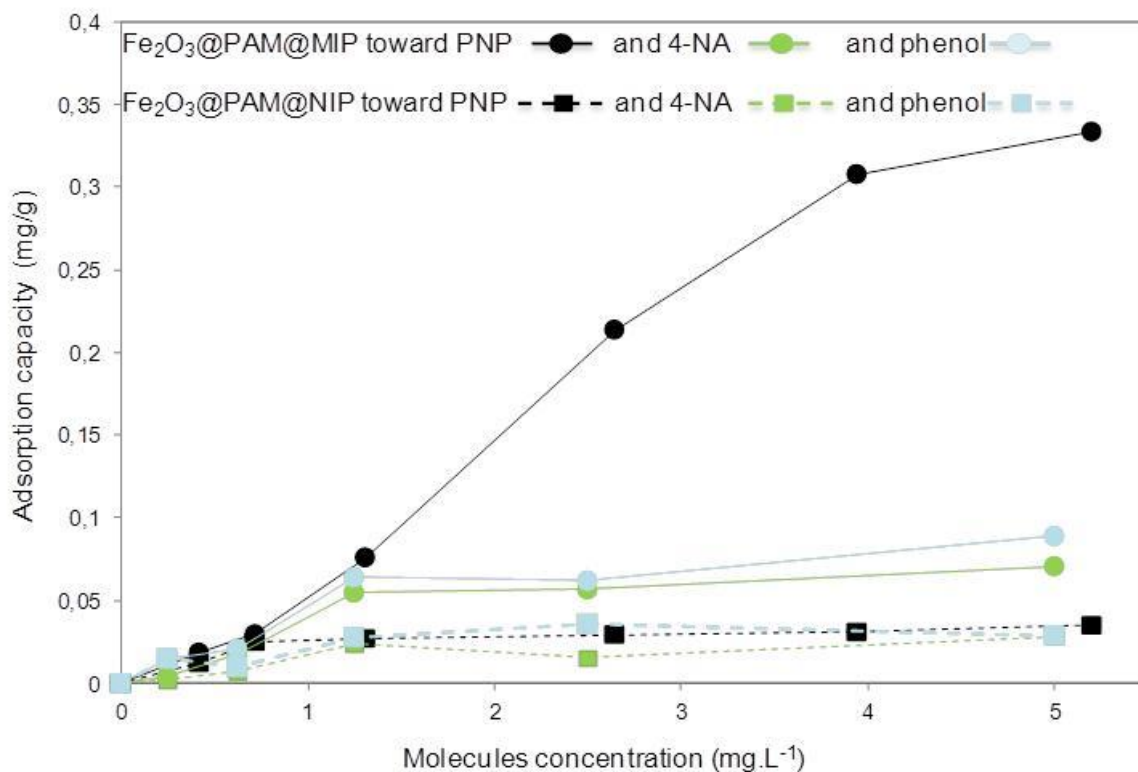


Figure 8. Adsorption isotherms of $\text{Fe}_2\text{O}_3@\text{PAM}@NIP$ and $\text{Fe}_2\text{O}_3@\text{PAM}@MIP$ toward paranitrophenol (PNP), 4-nitroaniline (4-NA) and phenol.

The recognition properties of the MIP were evaluated by equilibrium binding experiments with PNP. PNP (0.4 to 5.2 mg.L⁻¹) was incubated with Fe₂O₃@PAM@MIP (and @NIP) in water at pH 5.5. After 1h incubation, the solutions were dialyzed and the amount of free PNP was quantified by UV/Vis spectroscopy. The recognition of PNP (Figure 8) is specific, since binding to the MIP ($Q_{\max} = 0.36 \text{ mg.g}^{-1}$) is much higher than with the control NIP ($Q_{\max} = 0.058 \text{ mg.g}^{-1}$). These results indicate that the MIP containing imprinted cavities are highly selective to target PNP. To determine the binding selectivity of Fe₂O₃@MIP for PNP, 4-nitroalinine (4-NA) and phenol were selected as an interfering molecule since their molecular structure is quite similar to PNP. The results, displayed in Figure 8, show that Fe₂O₃@MIP exhibit good adsorption selectivity for the template PNP with a higher binding capacity for PNP than for 4-NA ($Q_{\max} = 0.081 \text{ mg.g}^{-1}$) and phenol ($Q_{\max} = 0.096 \text{ mg.g}^{-1}$). Fe₂O₃@NIP NP present the same low adsorption capacity for 4-NA ($Q_{\max} = 0.029 \text{ mg.g}^{-1}$) and phenol ($Q_{\max} = 0.027 \text{ mg.g}^{-1}$) than for PNP.

3.5. AMF for regeneration of the NP. We previously showed that AMF can be used to destabilize the weak interactions existing between the MIP and the template.⁷ The same principle is applied here for the extraction of PNP from the MIP in order to recycle the magnetic materials by disrupting hydrogen bonds existing between the polymer and PNP. To evaluate the PNP release kinetic, nanoparticles of Fe₂O₃@PAM@MIP-PNP (3 mL, 20 mg) were placed under AMF (342 KHz, 9 mT) for 10, 15, 20, 25 and 30 min. The Fe₂O₃@PAM@MIP-PNP NP, submitted to the AMF, released 0.12 mg g⁻¹ of PNP after 30 min at 25 °C (inset of Figure 9 and the first blue square in Figure 9). Then the NP were recovered and mixed during 1h with a 6 mg L⁻¹ solution of PNP, corresponding to the maximal absorption concentration (Figure 8), and the supernatant analysis leads to a total concentration of adsorbed PNP in the MIP of 0.225 mg.g⁻¹

(the first red square in Figure 9). After AMF pulse on the same sample, a released concentration of 0.11 mg.g^{-1} is reached again. The release of about 50% of the amount of PNP loaded may be due to the temperature gradient in the polymer. Actually, the polymer close to the surface of the particles is affected by the temperature increase and the hydrogen bonds are broken and the PNP is released, the PNP far from the particles is not released. The adsorption/desorption under AMF cycle was repeated three times without modification. After four adsorption/regeneration cycles, 0.22 mg.g^{-1} of PNP is adsorbed, which demonstrated the physical robustness and mechanically durability of the imprinted network. The possible reason for loss of absorption capacity ($Q_{\text{max}} = 0.36 \text{ mg.g}^{-1}$) is that some recognition sites in $\text{Fe}_2\text{O}_3@\text{PAM}@MIP$ are jammed after regeneration or destroyed by AMF application. Nevertheless, the results show that the reusability of $\text{Fe}_2\text{O}_3@\text{PAM}@MIP$ is satisfactory, with a constant release capacity.

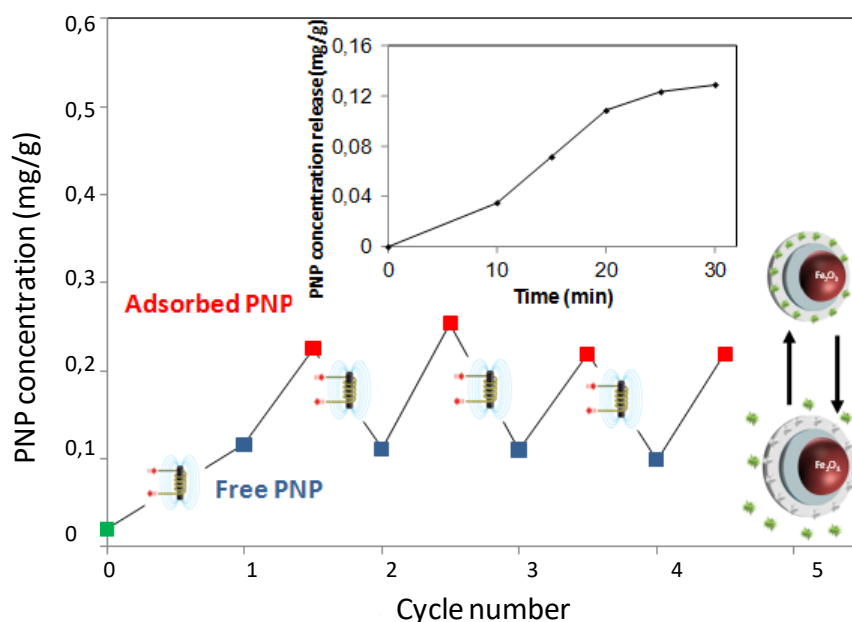


Figure 9. Cycles of PNP adsorption (red square) and release under AMF (blue square) for $\text{Fe}_2\text{O}_3@\text{PAM}@MIP$ -PNP. Green squares represent the PNP passive release from the particles. Inset represents the dynamic release curve of paranitrophenol PNP under AMF.

4. CONCLUSIONS

In summary, we showed that it is possible to use iron oxide nanoparticles as hot spots to induce polymerization of polymer layers on iron oxide nanoparticles surface, and to remove the adsorbed molecule from the molecularly imprinted polymer network. The nanoplatform provided excellent efficiency for adsorption of targeted pollutants, and heat-controlled release of the pollutant molecules for recycling. Our approach offers several advantages over conventional methods: (i) polymerization is induced at the surface of nanoparticles; (ii) ease and rapidity of surface functionalization of magnetic nanoparticles with different types of polymers under AMF; (iii) formation of well-dispersed nanoparticles; (iv) formation of multiple polymer shells under consecutive AMF applications. Then, AMF was successfully used to release PNP previously adsorbed, thus recycling the magnetic material. This unprecedented synthetic approach could provide a versatile strategy for magnetic nanoparticles functionalization through the magnetically induced in situ grafting of multiple layers of polymer shells. Other magnetic nanoparticles that have heating conversion properties would similarly enhance the polymerization conversion rate and other chemical reactions could be envisaged to produce unique materials.

Supporting Information. The following files are available free of charge. Size distribution from DLS of γ -Fe₂O₃ nanoparticles and Fe₂O₃@PAM synthesized without TTMA at 342kHz, 9mT; FT-IR spectra of Fe₂O₃@TTMA and Fe₂O₃@PAM synthesized at 18 mT and different frequencies; FT-IR spectra of Fe₂O₃@PAM nanoparticles synthesized at 342kHz, 18mT and Fe₂O₃@PAM nanoparticles synthesized at 342kHz, 9mT; FT-IR spectra of Fe₂O₃@PAM nanoparticles synthesized at 342kHz, 18mT after 10min, 20min and 30min; High resolution TEM images of Fe₂O₃@PAM_{AMF} nanoparticles and Fe₂O₃@PAM_T; Thermogravimetric analysis of Fe₂O₃@PAM@NIP nanoparticles; Calibration curve of PNP;

Magnetization curves obtained by vibrating sample magnetometer at room temperature of Fe₂O₃ nanoparticles(PDF).

AUTHOR INFORMATION

Corresponding Author

* Nebewia Griffete, Sorbonne Universités, UPMC Univ Paris 06, CNRS, Laboratoire PHENIX, Case 51, 4 place Jussieu, F-75005 Paris, France.

Email: nebewia.griffete@upmc.fr

Author Contributions

The manuscript was written through contributions of all authors. All authors have given approval to the final version of the manuscript.

Funding Sources

Espinosa acknowledges the Intra-European Project FP7-PEOPLE-2013-740 IEF-62647.

ACKNOWLEDGMENT

We kindly acknowledge Aude Michel for the TEM pictures. We also thank Delphine Talbot for the ATG characterization of the nanomaterials.

REFERENCES

- (1) Mornet, S.; Vasseur, S.; Grasset, F.; Duguet, E. Magnetic Nanoparticle Design for Medical Diagnosis and Therapy *J. Mater. Chem.* **2004**, *14*, 2161-2175.
- (2) Gallo, J.; Long, N.J.; Aboagye, E.O. Magnetic Nanoparticles as Contrast Agents in the Diagnosis and Treatment of Cancer *Chem. Soc. Rev.* **2013**, *42*, 7816-7833.

- (3) Gu, H.; Xu, K.; Xu, C.; Xu, B. Biofunctional Magnetic Nanoparticles for Protein Separation and Pathogen Detection *Chem. Commun.* **2006**, *9*, 941-949;
- (4) Niemeier, C.M. Nanoparticles, Proteins, and Nucleic Acids: Biotechnology Meets Materials Science *Angew. Chem. Int. Ed.* **2001**, *40*, 4128-4158.
- (5) Kakwere, H.; Leal, M.P.; Materia, M.E.; Curcio, A.; Guardia, P.; Niculaes, D.; Marotta, R.; Falqui A.; Pellegrino, T. Functionalization of Strongly Interacting Magnetic Nanocubes with (Thermo)Responsive Coating and Their Application in Hyperthermia and Heat-Triggered Drug Delivery *ACS Appl. Mater. Interfaces* **2015**, *7*, 10132-10145.
- (6) Jae-Hyun, L.; Kyuri, L.; Seung Ho, M.; Yuhan, L.; Tae Gwan P.; Jinwoo C. All-in-One Target-Cell-Specific Magnetic Nanoparticles for Simultaneous Molecular Imaging and siRNA Delivery *Angew. Chem. Int. Ed.* **2009**, *48*, 4174-4179.
- (7) Griffete, N.; Fresnais, J.; Espinosa, A.; Wilhelm, C.; Bee, A.; Ménager, C., Design of Magnetic Molecularly Imprinted Polymer Nanoparticles for Controlled Release of Doxorubicin under an Alternating Magnetic Field in Athermal Conditions *Nanoscale*, **2015**, *7*, 18891-18896.
- (8) Shah, S.A.; Majeed, A.; Shafique, M.A.; Rashid K.; Awan, S.U. Cell Viability Study of Thermo-Responsive Core-Shell Superparamagnetic Nanoparticles for Multimodal Cancer Therapy *Appl. Nanosci.*, **2014**, *4* 227-232.
- (9) Patra, S.; Roy, E.; Karfa, P.; Kumar, S.; Madhuri R.; Sharma, P.K. Dual-Responsive Polymer Coated Superparamagnetic Nanoparticle for Targeted Drug Delivery and Hyperthermia Treatment *ACS Appl. Mater. Interfaces*, **2015**, *7*, 9235-9246.
- (10) Jung, J.H.; Lee, J. H., Shinkai, S. Functionalized Magnetic Nanoparticles as Chemosensors and Adsorbents for Toxic Metal Ions in Environmental and Biological Fields *Chem. Soc. Rev.* **2011**, *40*, 4464-4474.

- (11) Griffete, N.; Li, H.; Lamouri, A.; Redeuilh, C.; Chen, K.; Dong, C.Z.; Nowak, S.; Ammar S.; Mangeney C. Magnetic Nanocrystals Coated by Molecularly Imprinted Polymers for the Recognition of Bisphenol A *J. Mater. Chem.* **2012**, *22*, 1807-1811.
- (12) Fortin, J.P.; Wilhelm, C.; Servais, J.; Menager, C.; Bacri J.C.; Gazeau F. Size-Sorted Anionic Iron Oxide Nanomagnets as Colloidal Mediators for Magnetic Hyperthermia *J. Am. Chem. Soc.* **2007**, *129*, 2628-2635.
- (13) Yu, M.; Jeong, Y.; Park, J.; Park, S.; Kim, J.; Min, J.; Kim K.; S. Jon, Drug-Loaded Superparamagnetic Iron Oxide Nanoparticles for Combined Cancer Imaging and Therapy In Vivo *Angew. Chem. Int. Ed.* **2008**, *47*, 5442–5445.
- (14) Neuberger, T.; Schopf, B.; Hofmann, H.; Hofmann M.; Von Rechenberg, B. Superparamagnetic Nanoparticles for Biomedical Applications: Possibilities and Limitations of a New Drug Delivery System *J. Magn. Magn. Mater.* **2005**, *293*, 483-496.
- (15) Xie, J.; Chen, K.; Lee, H.; Xu, C.; Hsu, A.R.; Peng, S.; Chen, X.; Sun, S. Ultrasmall c(RGDyK)-Coated Fe₃O₄ Nanoparticles and Their Specific Targeting to Integrin $\alpha v \beta 3$ -Rich Tumor Cells *J. Am. Chem. Soc.*, **2008**, *130*, 7542-7543.
- (16) Mehdaoui, B.; Tan, R.P.; Meffre, A.; Carrey, J.; Lachaize, S.; Chaudret, B.; Respaud, M. Increase of Magnetic Hyperthermia Efficiency due to Dipolar Interactions in Low-Anisotropy Magnetic Nanoparticles: Theoretical and Experimental Results *Phys. Rev. B* **2013**, *87*, 174419.
- (17) Sanson, C.; Diou, O.; Thévenot, J.; Ibarboure, E.; Soum, A.; Brûlet, A.; Miraux, S.; Thiaudière, E.; Tan, S.; Brisson, A.; Dupuis, V.; Sandre, O.; Lecommandoux, S. Doxorubicin Loaded Magnetic Polymersomes: Theranostic Nanocarriers for MR Imaging and Magneto-Chemotherapy. *ACS Nano* **2011**, *5*, 1122–1140.

- (18) Luk, B. T.; Zhang, L. Current Advances in Polymer-Based Nanotheranostics for Cancer Treatment and Diagnosis. *ACS Appl.Mater. Interfaces* **2014** , 6, 21859–21873.
- (19) Hemery , G.; Genevois, C.; Couillaud, F.; Lacomme, S.; Gontier, Ibarboure, E.E.; Lecommandoux, S.; Garanger E.; Sandre O. Monocore vs. Multicore Magnetic Iron Oxide Nanoparticles: Uptake by Glioblastoma Cells and Efficiency for Magnetic Hyperthermia *Mol. Syst. Des. Eng.* **2017**, 2, 629-639
- (20) Périgo, E.A.; Hemery, G.; Sandre, O; Ortega, D.; Garaio, E.; Plazaola, F. and F. J. Teran Fundamentals and advances in magnetic hyperthermia *Applied Physics Reviews* **2015**, 2, 041302.
- (21) Abramson, S.; Srithammavanh, L.; Siaugue, J.M.; Horner, O.; Xu X.; V. Cabuil, Nanometric core-shell-shell γ -Fe₂O₃/SiO₂/TiO₂ particles *J. Nanoparticle Res.* **2009**, 11, 459-465.
- (22) Chanteau, B.; Fresnais J.; Berret, J.F. Electrosteric Enhanced Stability of Functional Sub-10 nm Cerium and Iron Oxide Particles in Cell Culture Medium *Langmuir*, **2009**, 25, 9064-9070.
- (23) Stöber, W.; Fink A.; Bohn, E. Controlled Growth of Monodisperse Silica Spheres in the Micron Size Range *J. Colloid Interface Sci.* **1968**, 26, 9064-9070.
- (24) Kee Yi, D.; Selvan, S.T.; Seong Lee, S.; Papaefthymiou, G.C.; Kundaliya, D.; Ying J.Y. Silica-Coated Nanocomposites of Magnetic Nanoparticles and Quantum Dots *J. Am. Chem. Soc.* **2005**, 127, 4990-4991.
- (25) Santra, S.; Tapeç, R.; Theodoropoulou, N.; Dobson, J.; Hebard A.; Tan, W. Synthesis and Characterization of Silica-Coated Iron Oxide Nanoparticles in Microemulsion: The Effect of Nonionic Surfactants *Langmuir* **2001**, 17, 2900-2906.

- (26) Di Corato, R.; Quarta, A.; Piacenza, P.; Ragusa, A.; Figuerola, A.; Buonsanti, R.; Cingolani, R.; Manna, L.; Pellegrino, T. Water Solubilization of Hydrophobic Nanocrystals by Means of Poly(maleic anhydride-alt-1-octadecene) *J. Mater. Chem.* **2008**, *18*, 1991-1996.
- (27) Parak, W.G.J.; Lin, C.A.J.; Sperling, R.A.; Li, J.K.; Yang, T.Y.; Li, P.Y.; Zanella M.; Chang, W.H. Design of an Amphiphilic Polymer for Nanoparticle Coating and Functionalization *Small* **2008**, *4*, 334-341.
- (28) Padwal, P.; Bandyopadhyaya R.; Mehra S. Polyacrylic Acid-Coated Iron Oxide Nanoparticles for Targeting Drug Resistance in Mycobacteria *Langmuir* **2014**, *30*, 15266-15276.
- (29) Tassa, C.; Shaw, S.Y.; Weissleder, R. Dextran-Coated Iron Oxide Nanoparticles: A Versatile Platform for Targeted Molecular Imaging, Molecular Diagnostics, and Therapy *Acc. Chem. Res.* **2011**, *44*, 842-852.
- (30) Beyazit, S.; Ambrosini, S.; Marchyk, N.; Palo, E.; Kale, V.; Soukka, T.; Tse Sum Bui, B. Haupt, K. Versatile Synthetic Strategy for Coating Upconverting Nanoparticles with Polymer Shells through Localized Photopolymerization by Using the Particles as Internal Light Sources *Angew. Chem. Int. Ed.* **2014**, *53*, 8919-8923.
- (31) Darwish, M.S.A.; Stibor I. Preparation and Characterization of Magnetite–PDMS Composites by Magnetic Induction Heating *Materials Chemistry and Physics* **2015**, *15*, 163-169.
- (32) Miller, K.R.; Soucek, M.D. Magnetic Macro-initiators *J. Mater. Chem. C* **2015**, *3*, 9175-9190.
- (33) Haupt, K. Creating a Good Impression *Nature Biotechnol.* **2002**, *20*, 884-885.
- (34) Vlatais, G.; Andersson, L.I.; Muller R.; Mosbach, K. Drug Assay Using Antibody Mimics Made by Molecular Imprinting *Nature* **1993**, *361*, 645-653.

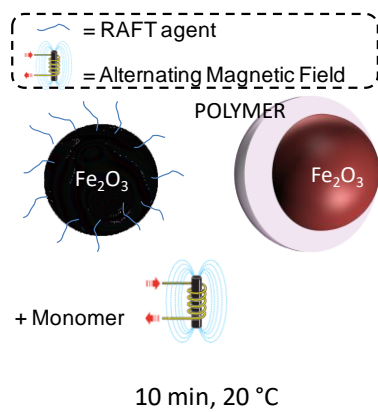
- (35) Linares, A.V.; Falcimaigne-Cordin, A.; Gheber L.A.; Haupt, K. Patterning Nanostructured, Synthetic, Polymeric Receptors by Simultaneous Projection Photolithography, Nanomolding, and Molecular Imprinting *Small* **2011**, *7*, 2318-2325.
- (36) Griffete, N.; Frederich, H.; Maitre, A.; Ravaine, S.; Chehimi M.M.; Mangeney, C. Inverse Opals of Molecularly Imprinted Hydrogels for the Detection of Bisphenol A and pH Sensing *Langmuir* **2012**, *28*, 1005-1012.
- (37) Griffete, N.; Frederich, H.; Maitre, A.; Schwob, C.; Ravaine, S.; Carbonnier, B.; Chehimi M.M.; Mangeney, C. Introduction of a Planar Defect in a Molecularly Imprinted Photonic Crystal Sensor for the Detection of bisphenol A *J. Colloid Interface Sci.* **2011**, *364*, 18-23.
- (38) Kazemi, S.; Sarabi, A.A.; Abdouss M. Synthesis and Characterization of Magnetic Molecularly Imprinted Polymer Nanoparticles for Controlled Release of Letrozole *Korean J. Chem. Eng.* **2015**, *1*, 3289–3297.
- (39) Massart, R. Preparation of Aqueous Magnetic Liquids in Alkaline and Acidic Media. *IEEE Trans. Magn.* **1981**, *17* (2), 1247–1248.
- (40) Piletsky, A.; Matuschewski, H.; Schedler, U.; Wilpert, A.; Piletska, E.V.; Thiele, T.A.; Ulbricht, M. Surface Functionalization of Porous Polypropylene Membranes with Molecularly Imprinted Polymers by Photograft Copolymerization in Water Sergey *Macromolecules*, **2000**, *33*, 3092–3098.
- (41) Haupt, K.; Mayes, A.G.; Mosbach K. Herbicide Assay Using an Imprinted Polymer-Based System Analogous to Competitive Fluoroimmunoassays *Anal. Chem.*, **1998**, *70*, 3936–3939.
- (42) Lefebure, S.; Dubois, E.; Cabuil, V.; Neveu S.; Massart, R. Monodisperse Magnetic Nanoparticles: Preparation and Dispersion in Water and Oils *J. Mat. Res.* **1998**, *13*, 2975-2981.

- (43) Cabuil, V.; Massart R.; Bacri, J.C.; Perzinski, R.; Salin, D. Ionic Ferrofluids : Towards Fractional Distillation *J.Chem. Research* **1987**, (5), 130.
- (44) Di Corato, R.; Espinosa, A.; Lartigue, L.; Tharaud, M.; Chat, S.; Pellegrino, T. ; Ménager, C.; Gazeau, F.; Wilhelm, C. Magnetic Hyperthermia Efficiency in the Cellular Environment for Different Nanoparticle Designs *Biomaterials* **2014**, 35, 6400-6411.
- (45) Douadi-Masrouki, S.; Frka-Petesic, B.; Save, M.; Charleux, B.; Cabuil, V.; Sandre, O. Incorporation of Magnetic Nanoparticles into Lamellar Polystyrene-b-poly(n-butyl methacrylate) Diblock Copolymer Films: Influence of the Chain End-Groups on Nanostructuration *Polymer* **2010**, 51, 4673-4685.
- (46) Robbes, A.S.; Cousin, F.; Meneau, F.; Chevigny, C.; Gimes, D.; Fresnais, J.; Schweins, R.; Jestin, J. Controlled Grafted Brushes of Polystyrene on Magnetic γ -Fe₂O₃ Nanoparticles via Nitroxide-Mediated Polymerization *Soft Matter*. **2012**, 8, 3407-3418.
- (47) Rocchiccioli-Deltcheff, C.; Franck, R.; Cabuil V.; Massart, R. Surfacted Ferrofluids: Interactions at the Surfactant-Magnetic Iron Oxide Interface. *J. Chem. Res.* **1987**, 5, 126-127.
- (48) Cornell R.M.; Schertmann, U. The Iron Oxides: Structure, Properties, Reactions, Occurrence and Uses, Wiley-VCH, Weinheim **1996**.
- (49) Shi, Y.; van den Dungen, E.T.A.; Klumperman, B.; van Nostrum C.F.; Hennink, W.E. Reversible Addition–Fragmentation Chain Transfer Synthesis of a Micelle-Forming, Structure Reversible Thermosensitive Diblock Copolymer Based on the *N*-(2-Hydroxy propyl) Methacrylamide Backbone *ACS MacroLett.* **2013**, 2, 403-408.
- (50) Wang, K.; Peng, H.; Thurecht, K.J.; Puttick S.; Whittaker, A.K. Segmented Highly Branched Copolymers: Rationally Designed Macromolecules for Improved and Tunable 19F MRI. *Biomacromolecules* **2015**, 16, 2827-2839.

- (51) Li, F.; Ye, L.; Li, Y.; Wu, T. Investigation into the Adsorption of Partially Hydrolyzed Polyacrylamide onto in situ Formed Magnesium Hydroxide Particles *RSC Adv.* **2016**, *6*, 31092-31100.
- (52) Palles, D.; Konidakis, I.; Varsamis C.P.E.; Kamitsos, E.I. Vibrational Spectroscopic and Bond Valence Study of Structure and Bonding in Al₂O₃-containing AgI–AgPO₃ glasses. *RSC Adv.* **2016**, *6*, 16697-16710.
- (53) Liu, X.H.; Xu, H.J.; Sun, S.Q.; Huang, J.; Li, G.Y.; Zhu, Y.; Gao, H.Y.; Zhang Z.C.; Wang, J.H. Analysis and Identification of Chinese Drugs by Three-step Infrared Spectroscopy—A case
- (54) Baalousha, M.; Manciuola, A.; Cumberl, S.; Kendall, K., Lead, J. R. Aggregation and Surface Properties of Iron Oxide Nanoparticles: Influence of pH and Natural Organic Matter *Anal. Methods* **2012**, *4*, 3344-3350.
- (55) Riedinger, A.; Guardia, P.; Curcio, A.; Garcia, M. A.; Cingolani, R.; Manna, L.; Pellegrino, T. Subnanometer Local Temperature Probing and Remotely Controlled Drug Release Based on Azo-Functionalized Iron Oxide Nanoparticles. *Nano Lett.* **2013**, *13*, 2399–2406.
- (56) Brites, C. D. S.; Lima, P. P.; Silva, N. J. O.; Millan, A.; Amaral, V.S.; Palacio, F.; Carlos, L. D. A Luminescent Molecular Thermometer for Long-Term Absolute Temperature Measurements at the Nanoscale. *Adv. Mater.* **2010**, *22*, 4499–4504.
- (57) Wulff, G. Molecular Imprinting in Cross-Linked Materials with the Aid of Molecular Templates— A Way towards Artificial Antibodies. *Angew. Chem., Int. Ed. Engl.* **1995**, *34*, 1812-1832.
- (58) Mosbach, K.; Ramstrom, O. Bio/Technology, the Emerging Technique of Molecular Imprinting and its Future Impact on Biotechnology, *Nature Biotechnology* **1996**, *14*, 163–170.

(59) Boitard, C.; Rollet, A.L.; Ménager C.; Griffete N. Surface-Initiated Synthesis of Bulk-Imprinted Magnetic Polymer for Protein Recognition. *Chem. Comm*, **2017**, 53, 8846-8849.

Table of contents graphic



Supporting Information

Thermal Polymerization on the Surface of Iron Oxide Nanoparticles Mediated by Magnetic Hyperthermia: Implications for Multi-Shell Grafting and Environmental Applications

**Nebewia Griffete^{†*}, Jérôme Fresnais[†], Ana Espinosa[‡], Dario Taverna[§], Claire Wilhelm[‡],
and Christine Ménager[†]**

[†] Sorbonne Universités, UPMC Univ Paris 06, CNRS, Laboratoire PHENIX, Case 51, 4 place Jussieu, F-75005 Paris, France.

Email: nebewia.griffete@upmc.fr

[‡] MSC, UMR CNRS 7057, University Paris Diderot, 75205 Paris cedex 13, France.

[§] Institut de Minéralogie, de Physique des Matériaux et de Cosmochimie (IMPMC), Sorbonne Universités - UPMC Univ. Paris 6, CNRS UMR 7590, IRD UMR 206, MNHN, 4 place Jussieu, F-75005 Paris, France.

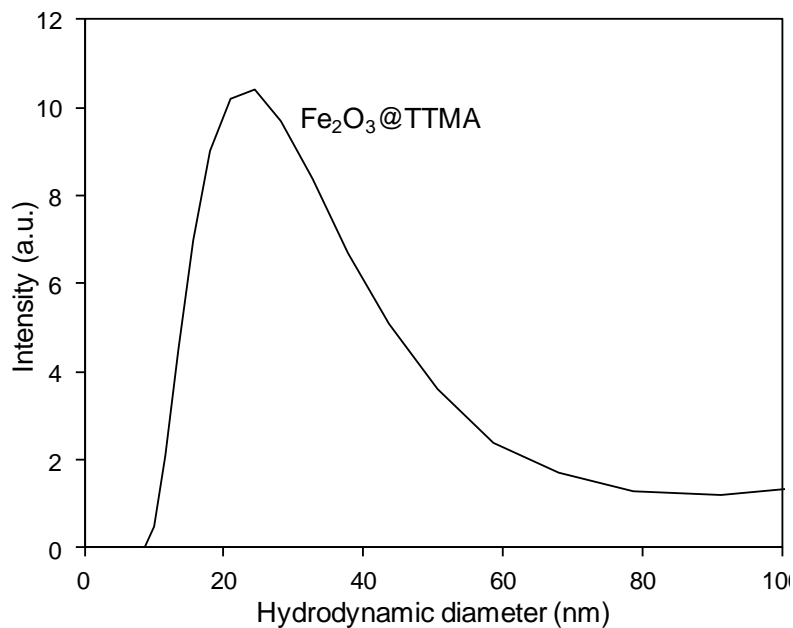


Figure S1. Size distribution from DLS (intensity average) of Fe₂O₃@TTMA nanoparticles diluted in water (pH=6) at a concentration of 0.05 mol.L⁻¹.

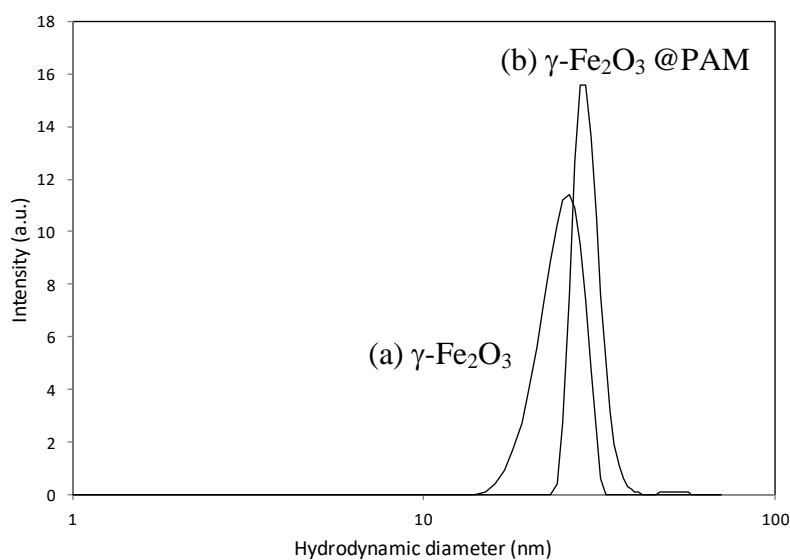


Figure S2. Size distribution from DLS (intensity average) of (a) γ -Fe₂O₃ nanoparticles and (b) Fe₂O₃@PAM synthesized without TTMA at 342kHz, 9mT and diluted in acidic water and water at a concentration of 0.05 mol.L⁻¹.

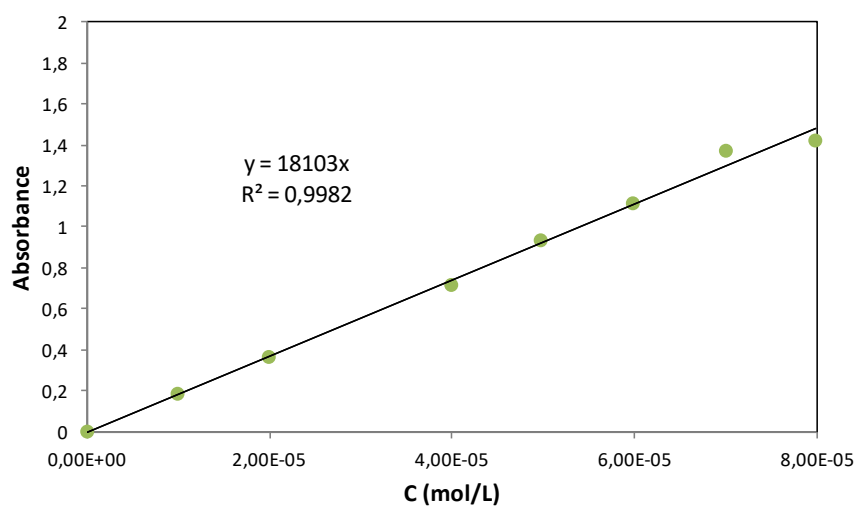


Figure S3. Calibration curve of PNP. The absorbance was measured at 400nm at pH = 10.

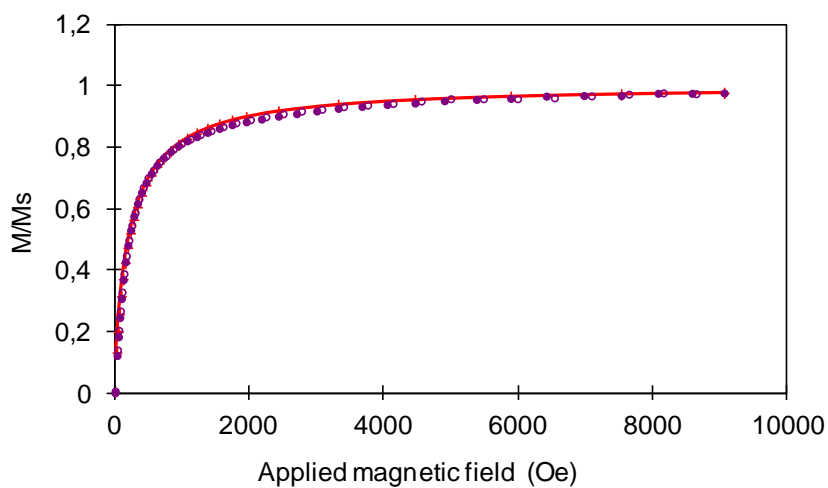


Figure S4. Magnetization curves obtained by vibrating sample magnetometer at room temperature of Fe₂O₃ nanoparticles.

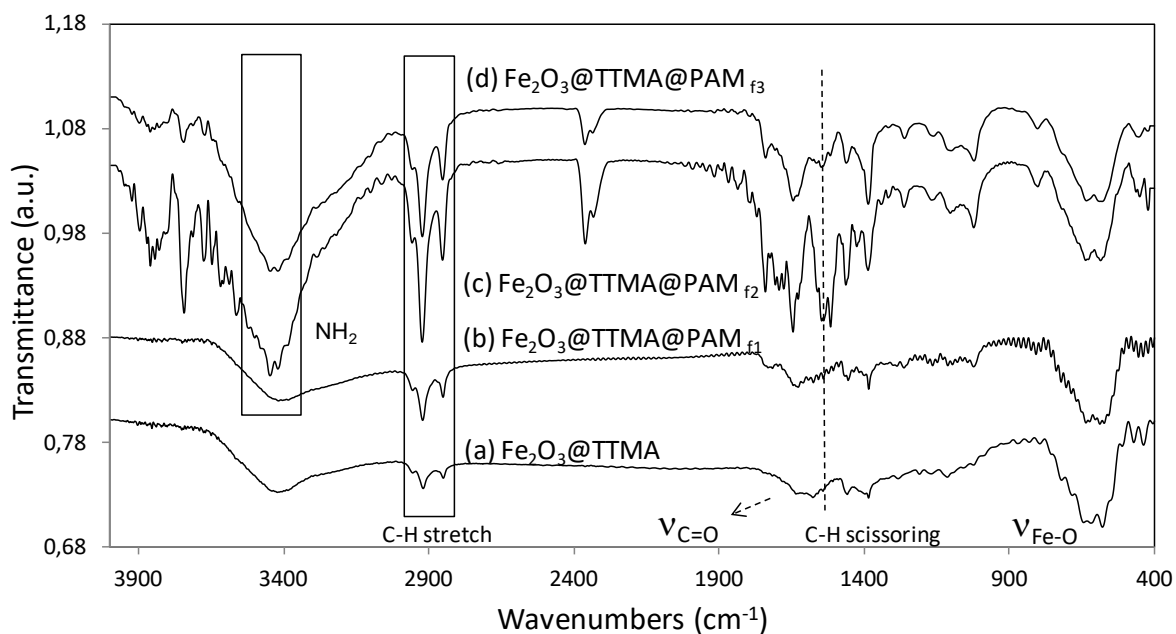


Figure S5. FT-IR spectra of (a) Fe₂O₃@TTMA, (b) Fe₂O₃@PAM synthesized at 18 mT and different frequencies (b) $f_1 = 144$ kHz, (c) $f_2 = 342$ kHz, and (d) $f_3 = 470$ kHz.

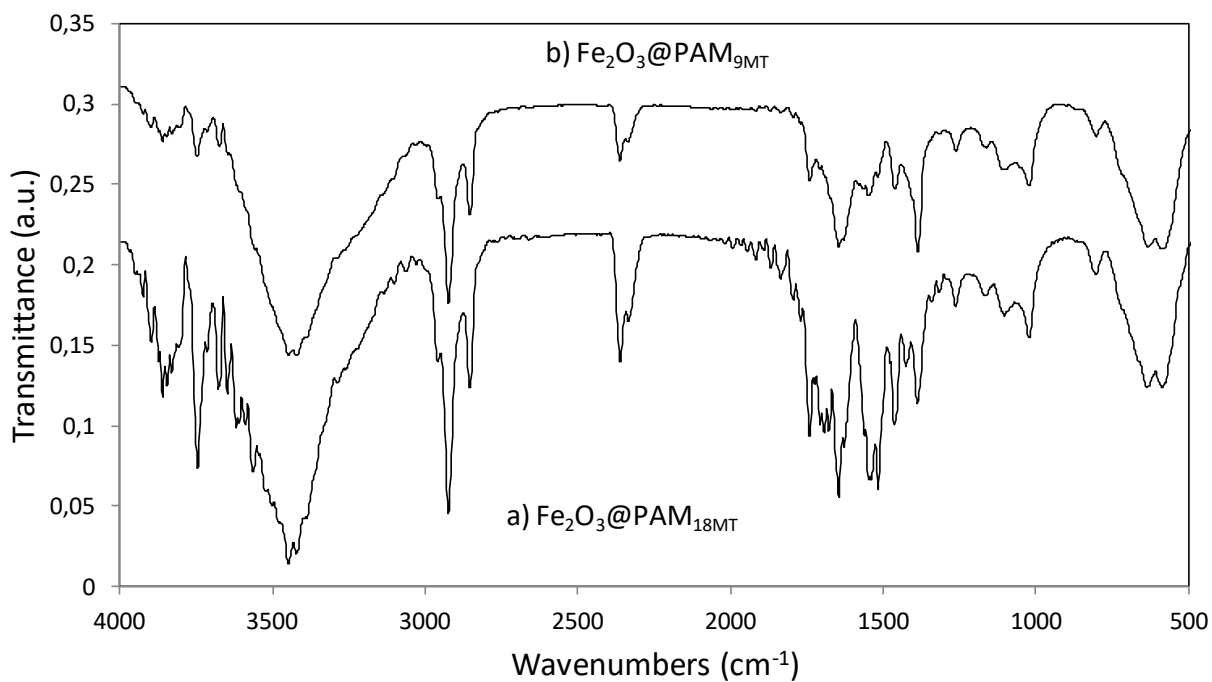


Figure S6. FT-IR spectra of (a) Fe₂O₃@PAM nanoparticles synthesized at 342kHz, 18mT and (b) Fe₂O₃@PAM nanoparticles synthesized at 342kHz, 9mT.

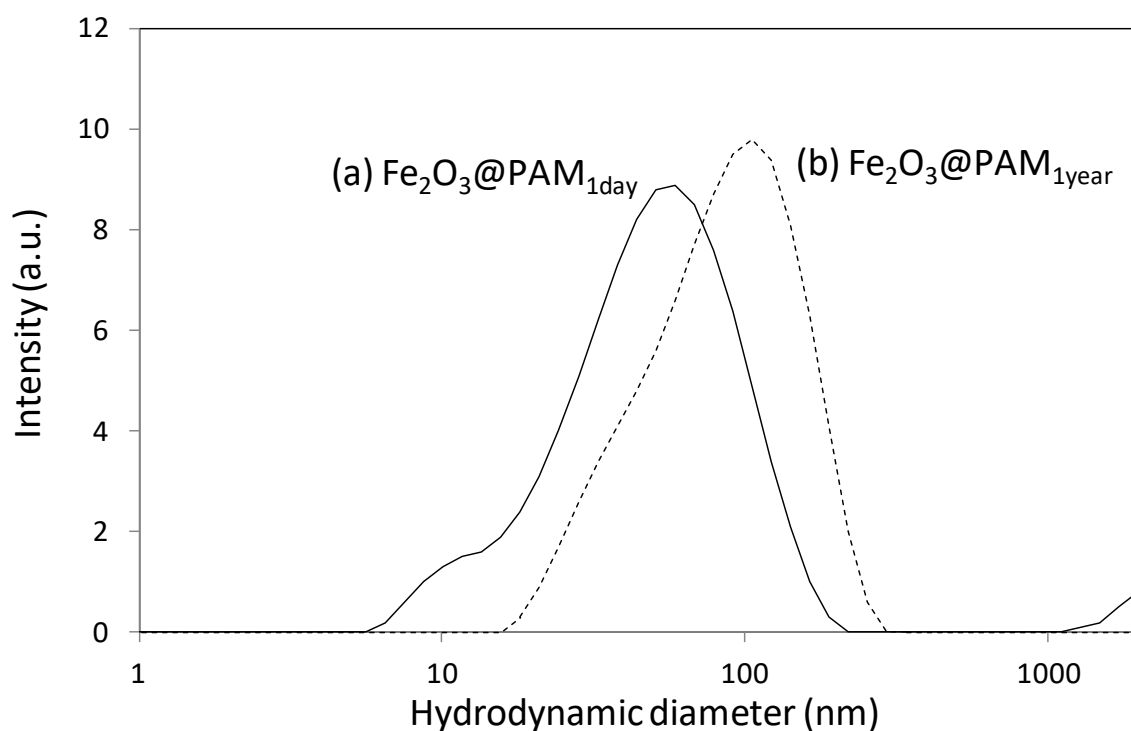


Figure S7. Hydrodynamic diameter measured by DLS (intensity average) of (a) $\text{Fe}_2\text{O}_3\text{@PAM}$ after the synthesis and (b) $\text{Fe}_2\text{O}_3\text{@PAM}$ NP 1 year after its synthesis diluted respectively in acidic water and in water at a concentration of approximately 0.05 mol.L^{-1} .

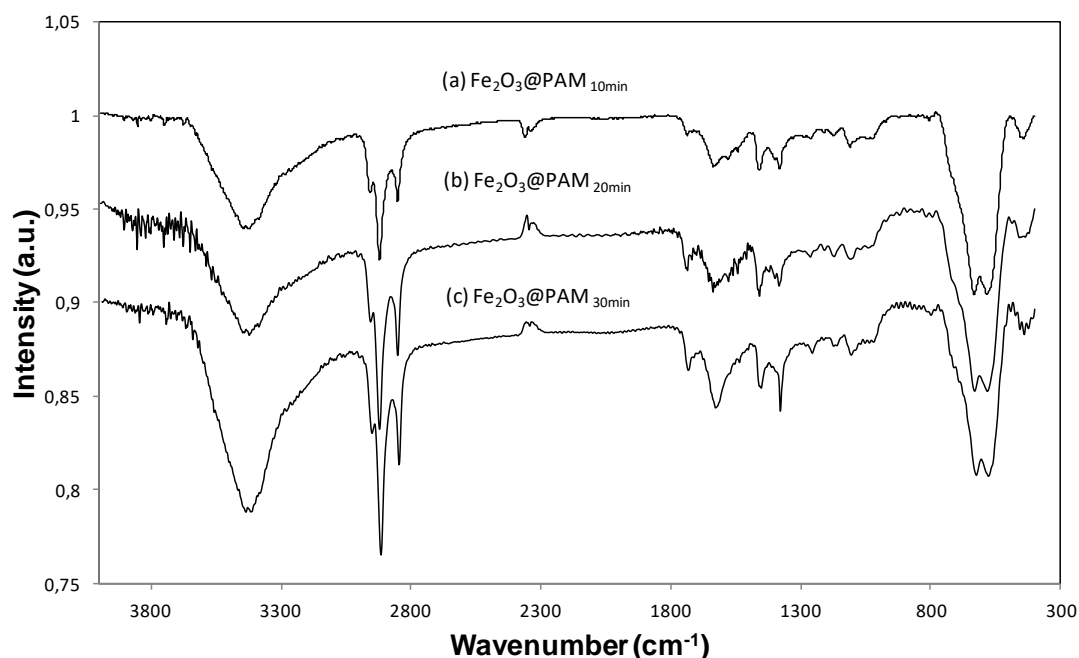


Figure S8. FT-IR spectra of $\text{Fe}_2\text{O}_3\text{@PAM}$ nanoparticles synthesized at 342kHz, 18mT after (a) 10min (b) 20min and (c) 30min.

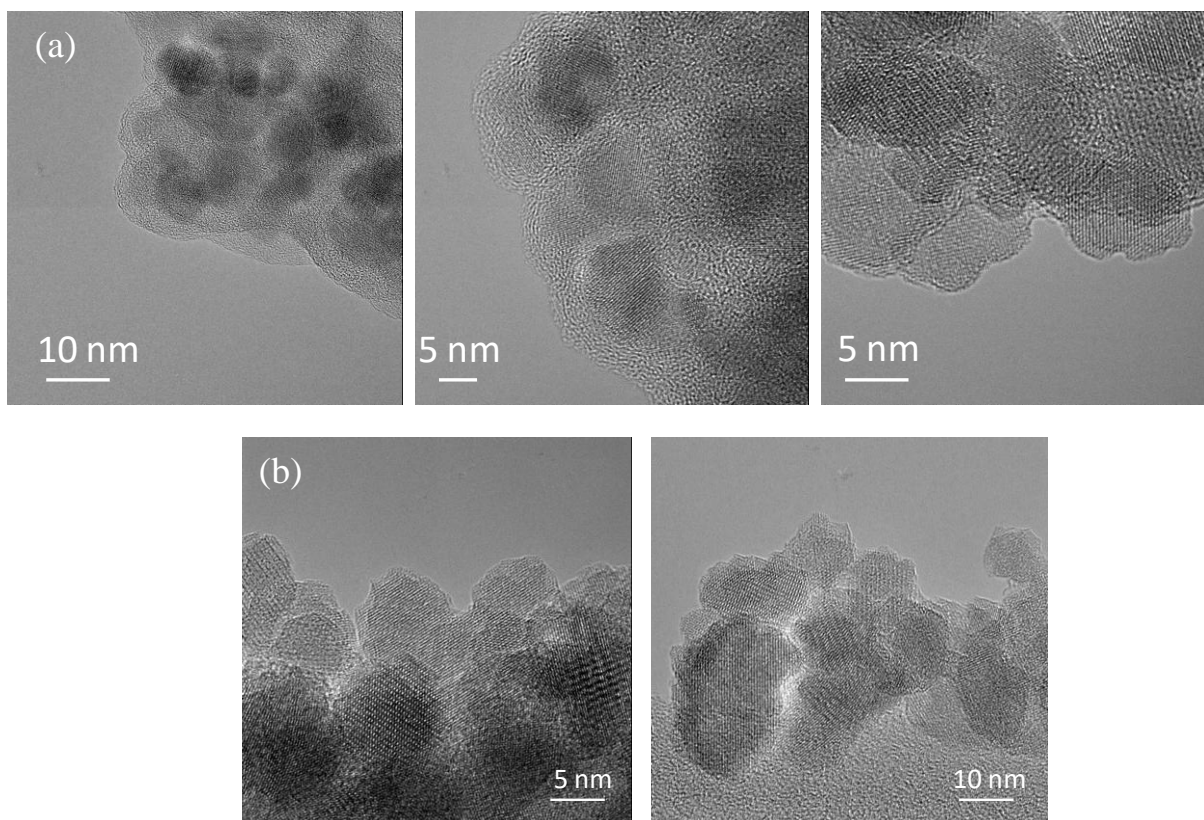


Figure S9. High resolution TEM images of a) $\text{Fe}_2\text{O}_3@PAM_{AMF}$ nanoparticles and b) $\text{Fe}_2\text{O}_3@PAM_T$.

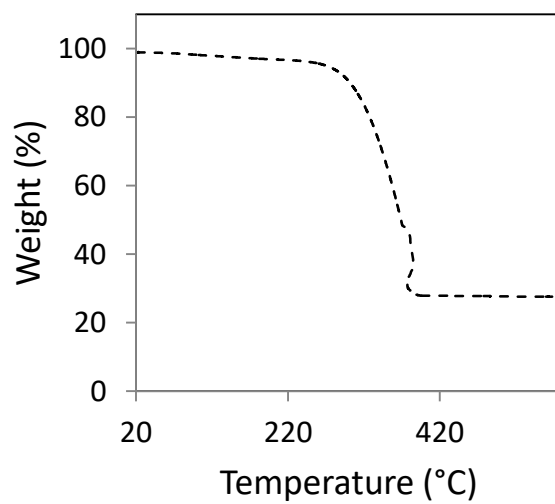


Figure S10. Thermogravimetric analysis of $\text{Fe}_2\text{O}_3@PAM@NIP$ nanoparticles.